
ROBMOT: ROBUST 3D MULTI-OBJECT TRACKING BY OBSERVATIONAL NOISE AND STATE ESTIMATION DRIFT MITIGATION ON LIDAR POINTCLOUD

Mohamed Nagy

Electrical and Computer Engineering
Khalifa University
mohamed.nagy@ieee.org

Naoufel Werghi

Electrical and Computer Engineering
Khalifa University
naoufel.werghi@ku.ac.ae

Bilal Hassan

Electrical and Computer Engineering
Khalifa University
bilal.hassan@ku.ac.ae

Jorge Dias

Electrical and Computer Engineering
Khalifa University
jorge.dias@ku.ac.ae

Majid Khonji

Electrical and Computer Engineering
Khalifa University
majid.khonji@ku.ac.ae

October 7, 2024

ABSTRACT

This work addresses limitations in recent 3D tracking-by-detection methods, focusing on identifying legitimate trajectories and addressing state estimation drift in Kalman filters. Current methods rely heavily on threshold-based filtering of false positive detections using detection scores to prevent ghost trajectories. However, this approach is inadequate for distant and partially occluded objects, where detection scores tend to drop, potentially leading to false positives exceeding the threshold. Additionally, the literature generally treats detections as precise localizations of objects. Our research reveals that noise in detections impacts localization information, causing trajectory drift for occluded objects and hindering recovery. To this end, we propose a novel online track validity mechanism that temporally distinguishes between legitimate and ghost tracks, along with a multi-stage observational gating process for incoming observations. This mechanism significantly improves tracking performance, with a 6.28% in HOTA and a 17.87% increase in MOTA. We also introduce a refinement to the Kalman filter that enhances noise mitigation in trajectory drift, leading to more robust state estimation for occluded objects. Our framework, RobMOT, outperforms state-of-the-art methods, including deep learning approaches, across various detectors, achieving up to a 4% margin in HOTA and 6% in MOTA. RobMOT excels under challenging conditions, such as prolonged occlusions and tracking distant objects, with up to a 59% improvement in processing latency.

3D multi-object tracking (MOT) is one of the pillars of autonomous driving. It is responsible for determining the state of objects in the environment, including their spatial location and motion parameters like velocity and acceleration. Trajectory drift has been observed in state estimation of occluded objects in the top-performing state-of-the-art CasTrack [1], as shown in Figure 1, failing to recover objects under challenging tracking conditions like prolonged occlusion and distant objects as emphasized in Figure 7. Our investigation shows that this drift results from fluctuation noise attached to the incoming 3D detections from deep learning models, which tracking-by-detection methods rely on for object localization on LiDAR point clouds. This noise impacts the precision of state estimation for spatial location and motion parameters of occluded objects that ultimately leads to deviation from the actual motion trajectory.

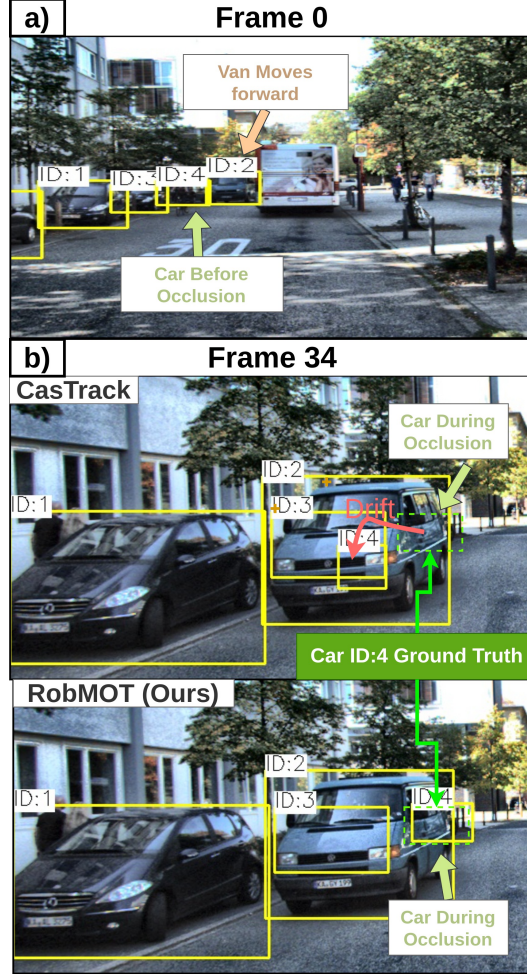


Figure 1: A trajectory drift scenario involving a car (ID4) hidden by a van (ID2). (a) At frame 0, four cars are detected and identified (ID1, ID2, ID3, ID4). (b) By frame 34, the method CasTrack [1] incorrectly estimates the position of car ID4 due to state estimation drift. A dashed green rectangle indicates the actual position. (c) Our proposed approach, with its noise mitigation techniques, successfully localizes car ID4 accurately.

Another issue is the absence of trajectory legitimacy verification in the MOT literature [1, 2, 3, 4, 5, 6]. These works apply a fine-tuned threshold on detection scores of the detections provided by deep learning models to filter out false positive observations that cause ghost trajectories. This approach is not reliable as it can block observations that belong to legitimate trajectories while leaking false positive observations. Since observations of legitimate trajectories can inherit some of the false positive characteristics, such as low detection scores for distant and partial occlusion scenarios, the MOT methods need to validate trajectories based on the consistency and legitimacy of their historical observations instead.

In this work, we tackle the above-mentioned challenges through Kalman filter refinement to mitigate the trajectory drift noise, Section 2.2, and propose a novel online mechanism to validate and distinguish between legitimate and ghost trajectories based on studying the characteristics of ghost tracks, Section 2.3. Our proposed refinement shows consistency in tracking for occluded objects superior to the latest state-of-the-art approach, CasTrack, demonstrated in Figure 1 and Figure 7. Next, the proposed trajectory validity mechanism incorporates a multi-stage observational gate that allows potential detections of legitimate tracks to pass to the system and an uncertainty formulation used to quantify the temporal improvement of trajectory certainty based on ghost track characteristics. The mechanism shows a 4% and 6% enhancement in HOTA and MOTA metrics, respectively.

We present the above innovative aspects within a 3D MOT tracking framework dubbed RobMOT. Our contribution can be summarized as follows:

1. To the best of our knowledge, this is the first work to uncover the trajectory drift noise associated with detections and its impact on the state estimation of occluded objects in 3D MOT. *Our refinement in Kalman filter shows superior performance over the top-performing benchmark, CastTrack [1], on challenging MOT conditions, demonstrated in Figure 7.*
2. We propose a novel online trajectory validity mechanism for temporal distinguishing between ghost and legitimate tracks, supported by a multi-stage observational gate for potential observation identification of the legitimate tracks. *The mechanism reduces about 80% of ghost tracks and enhances HOTA by 7%, as demonstrated in the ablation study Section 3.2.2.*
3. We propose an online 3D MOT framework with exceptional tracking performance, surpassing recent benchmarks to show its robustness across different datasets and detectors. *The tracking performance margin of our framework with the state-of-the-art CasTrack [1] reaches 4% in HOTA and 6% in MOTA, and the enhancement in computational latency is up to 53%, as demonstrated in Figure ??.*

1 Related Work

3D MOT methods on LiDAR point cloud could be categorized into learning and non-learning (classical) approaches. Part of learning-based methods in the literature involves end-to-end deep learning models that combine object detection and tracking [7, 8, 9, 10]. Meanwhile, other methods adapt tracking-by-detection paradigm [11, 12, 13, 14] when the detection of objects is given and the aim is to perform temporal tracking of the objects. The recent research integrates attention mechanism and transformers concepts [15, 16] into MOT to enhance the tracking performance. However, learning-based solutions require evolved hardware to be applicable to real-time applications.

Meanwhile, classical MOT solutions [4, 5, 2, 3, 6, 17, 1] have gained much attention due to their low latency and the comparative performance with learning-based solutions. Despite recent advancements in the classical methods, challenges such as the limitations of the Kalman filter, ghost tracks, and memory management persist, especially in autonomous driving applications where the environment constantly changes. We will shed light on these challenges and discuss the remedies proposed in the literature next.

Kalman filter (KF) is widely used in tracking-by-detection methods [2, 3, 17, 1] for autonomous driving because of its performance in filtering noise from state estimation while dealing with noisy measurements. If the noise is not properly modeled in the filter, it can cause deviation in the state estimation, as the filter’s estimation is sensitive to imprecise measurements. Cao et al. [6] prevent error accumulation in state prediction caused by periodic occlusion of objects by refining the object’s trajectory after object reappearance. However, the object should be recovered in order to refine its trajectory. Moreover, as of the point cloud’s sparsity, the incoming detections from 3D detectors suffer from spatial distortion around the object’s actual location. This spatial distortion results in an imprecise estimation of the motion parameters, ultimately leading to a deviation in the state estimation once the object faces an occlusion.

Ghost tracks are false positive detections generating illusion tracks that could eventually lead to wrong navigation of the AV. Since the tracking-by-detection paradigm relies heavily on detection accuracy, ghost tracks in object tracking can significantly harm the tracking performance. Kim et al. [3] introduce a multi-stage data association method to overcome this issue by employing multiple detection sources. Nevertheless, they still depend on predefined thresholds to prevent false positives. The downside of a fine-tuned threshold while filtering ghost tracks is the potential of leaking false positive detections that exceed the threshold while blocking detections that belong to actual tracks. Other approaches [5, 2] incorporate a filtration step to address false positive detections. Wang.X et al. [2] confirm the legitimacy of a track when three consecutive detections of that track have been observed. In contrast, Wang.L et al. [5] select objects for the highest 30% detections in the confidence score. However, the assumptions provided by these solutions may not apply to all scenarios, particularly distant objects or objects subject to periodic occlusions.

Memory management plays a critical role in addressing false positive detections. Maintaining ghost tracks in memory can lead to invalid associations. Meanwhile, early elimination may lose legitimate tracks under prolonged occlusion. In the literature, some work [2, 3, 5, 6] set up a threshold to discard tracks from memory based on how long these tracks have not been observed. Although short memory is suitable for ghost track elimination, it could also remove tracks of objects facing prolonged occlusion. On the other hand, long memory will not remove ghost tracks while increasing the computational time. Nagy et al. [17] attempt to address the trade-off by proposing an MOT solution with low latency and leveraging speed to extend the lifetime of objects, thus capturing more occlusion scenarios. While this approach excels in tracking objects with prolonged occlusion, it does not handle false positives. Wu et al. [1] resolve the issue by associating a confidence score to pre-observed objects in object association. This score decreases over time when the object becomes not observed for a period of time to prevent potential associations with false positive detections. Nonetheless, this approach cannot recover objects under prolonged occlusion as their association score will decrease. This work proposes RobMOT, a framework to mitigate state estimation deviation caused by fluctuation noise. It also provides adaptive identification for ghost tracks with a quick elimination from memory alongside a mechanism that prevents legitimate track detections from being blocked while filtering ghost tracks.

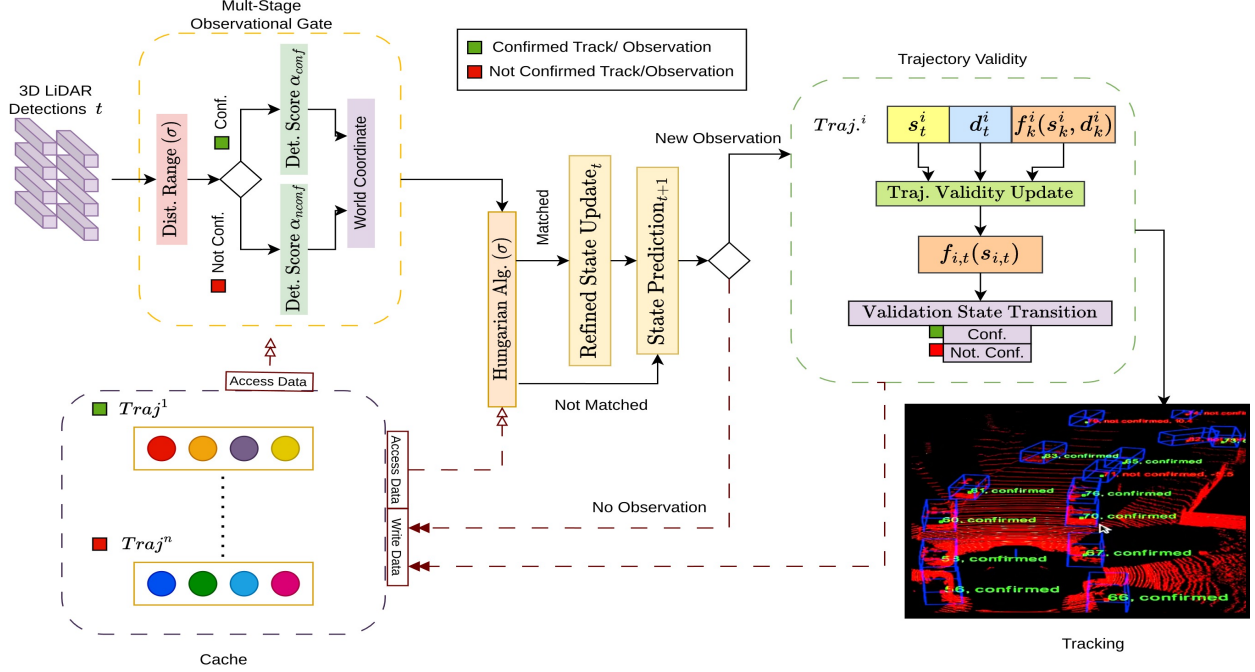


Figure 2: The RobMOT framework consists of four modules: a **multi-stage observational gate** for identifying legitimate observations, an **association trajectory innovation** for trajectories’ association with observations and next-state prediction, a **trajectory validity** for temporal validation of the trajectories, and a **cache** for storing and termination.

2 Methodology

As shown in Figure 2, the framework consists of four parts. **A multi-stage observational gate**: responsible for identifying potential observations of legitimate tracks. **Refined Kalman filter for noise mitigation**: a refined KF that updates the state estimation of cached trajectories and predicts their next state. **Trajectory validity**: Updates the legitimacy uncertainty of trajectories recently associated to observations. **Cache**: Holds trajectories stored in the framework and discards terminated tracks.

2.1 Multi-Stage Observational Gate

The multi-stage observational gate is an identification step for potential observations of the legitimate tracks identified by the trajectory validity stage, (see Section 2.3). The primary purpose of this stage is to allow observations of distant and partially occluded objects with low detection scores to enter while preventing overwhelming the system.

There are three types of the observations: observations of existing legitimate tracks, observations of tracks not generated yet by the system, and false observations that cause ghost tracks. Despite ghost tracks identification in the trajectory validity stage, discussed in Section 2.3, a threshold α_{nconf} should be assigned to the incoming observation to prevent overloading the MOT method because 3D deep learning detectors on LiDAR point cloud deliver immense number of detections with various detection scores. Thus, α_{nconf} is assigned a minimal value for detection scores to avoid overloading the system, regardless of the observations’ legitimacy, as this will be assessed later during the trajectory validity stage.

Even though assigning α_{nconf} with a small value allows a high volume of observations to pass to the system, it could block legitimate observations. Hence, We initially identify potential observations of existing legitimate tracks using the same Ecludian distance threshold σ used in the association step (see Section 2.2). Observations located in a distance less than σ to a legitimate track, identified by the trajectory validity stage in Section 2.3, are considered legitimate observations. Although the identified potential legitimate observations can pass directly to the system, we have observed that it still causes high latency because of flooding detections from deep learning models on the point cloud. Thus, we provide an additional detection α_{conf} score filtration when $\alpha_{conf} \leq \alpha_{nconf}$ to allow legitimate observations to enter the system while preventing overloading the system. α_{nconf} and α_{conf} are fine-tuned so that no enhancement

in the tracking performance is observed since their preliminary purpose is to prevent overloading the system. Lastly, the filtered observations are projected from the LiDAR coordinate to the world coordinate. Algorithm 1 demonstrates these procedures in detail.

Algorithm 1 Multi-Stage Observational Gate

```

function MultiStageObservationalGate( $D, T, \sigma, \alpha_c, \alpha_n$ )
Input:
   $D$ : List of 3D detections from LiDAR
   $T$ : List of trajectories in the cache
   $\sigma$ : Euclidean distance threshold
   $\alpha_{conf}$ : Detection score threshold for potential confirmed observations
   $\alpha_{nconf}$ : Detection score threshold for non-confirmed observations
Output:
   $P$ : List of detections that passed the gate

   $P \leftarrow []$ 
  for each  $det$  in  $D$  do
    if  $det.score \leq \alpha_{conf}$  then
      continue
    end if
     $confirmed \leftarrow false$ 
    for each  $traj$  in  $T.getConfirmed()$  do
       $dist \leftarrow EuclideanDistance(det.center, traj.lastStateEst)$ 
      if  $dist \leq \sigma$  then
         $confirmed \leftarrow true$ 
        break
      end if
    end for
    if  $confirmed$  or  $det.score \geq \alpha_{nconf}$  then
       $detW \leftarrow FromLidarToWorld(det)$ 
      Add  $detW$  to  $P$ 
    end if
  end for
  return  $P$ 
end function

```

2.2 Refined Kalman filter for Noise Mitigation

The permitted observations are associated with trajectories cached in the framework. We use the Hungarian algorithm [18] with the algebraic association strategy followed in [17]. The association for an observation is performed by selecting a trajectory with the shortest Euclidean distance between the estimated state and the observation. When the shortest distance to an observation exceeds σ , a new trajectory is created for the observation.

The framework performs next-state estimation for all trajectories cached in the system. Trajectories associated with an observation will pass through state update and state prediction as demonstrated in Figure 2. Other trajectories will go directly through state prediction. The framework utilizes KF with a constant acceleration motion model.

We have observed drift in state estimation for objects encountering occlusion or leaving the sensor field of view (off-scene). This phenomenon is also observed in the literature, as displayed in Figure 1 when the estimated trajectory of a parked car with ID 4 drifts away from the expected location during the occlusion. Figure 3 shows another scenario when two parked cars with ID 0 and 2 drift from the actual position after being off-scene. Our investigation of the phenomenon concludes that this deviation is caused by trembling in detection bounding boxes around objects' locations, which results in illusion movement for these objects that eventually impacts state update and prediction in KF.

We model this noise using the algebraic deviation, shown in Equation 1, between the detected bounding boxes $z_{ij}^{det} = (x_{ij}, y_{ij})$ and the actual location of the objects $z_{ij}^{gt} = (x_{ij}, y_{ij})$ across k observations for N objects using KITTI

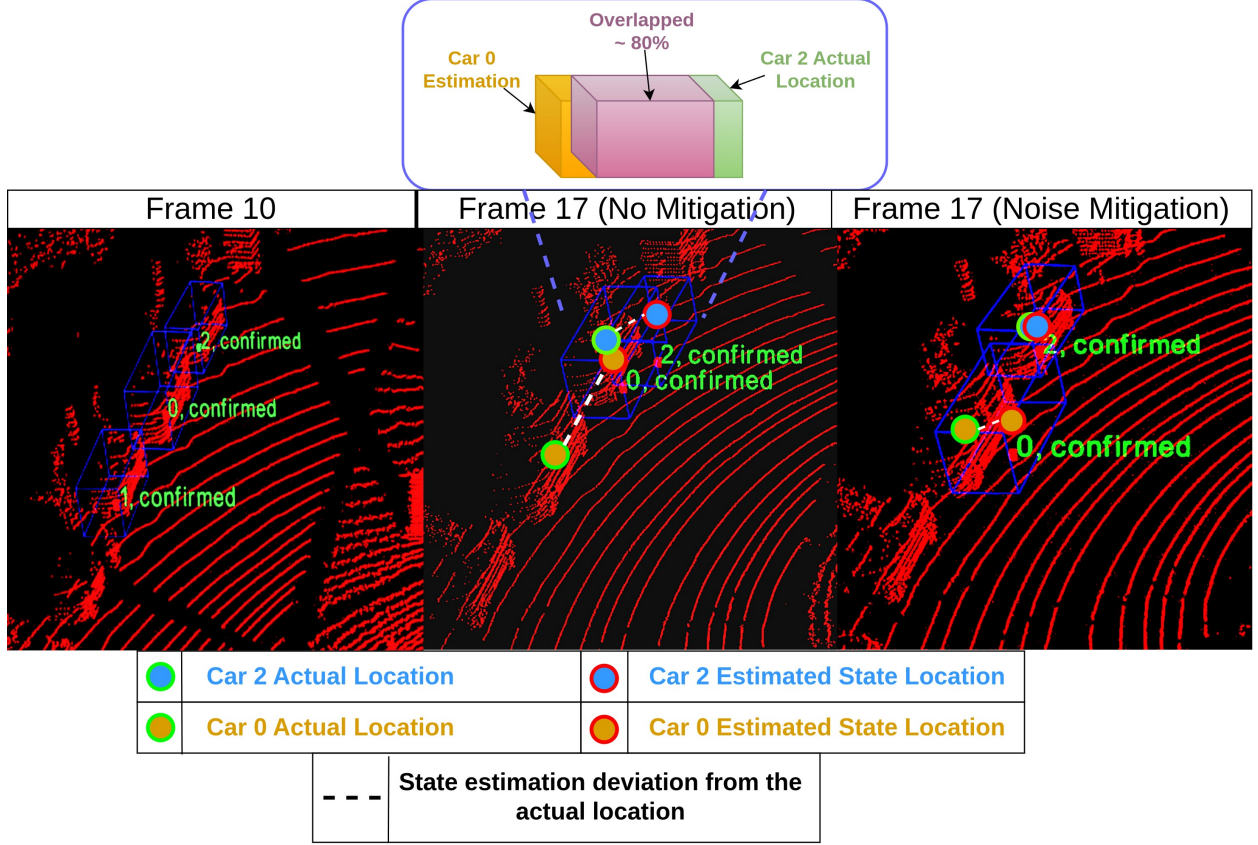


Figure 3: A scenario demonstrates the impact of detection noise on parked cars. Initially, the state estimation of the three cars is positioned correctly in frame 10. The middle frame, frame 17, shows drift in state estimation of cars with ID 0, **orange circle**, and 2, **blue circle**, caused by the noise. The state deviation from the original position of the cars is marked by **disconnected white line**. Considering the proposed noise mitigation (the third scene on the left), the state estimation of cars with ID 2 has no deviation, while the Car 0 deviation has been reduced significantly.

training dataset.

$$\mu_x = \frac{1}{\sum_{i=1}^N k_i} \sum_{i=1}^N \sum_{j=1}^{k_i} (z_{ij}^{gt}(x) - z_{ij}^{det}(x)) \quad (1)$$

$$\sigma_x^2 = \frac{1}{\sum_{i=1}^N k_i} \sum_{i=1}^N \sum_{j=1}^{k_i} ((z_{ij}^{gt}(x) - z_{ij}^{det}(x)) - \mu_x)^2$$

As depicted in Figure 4, the error distribution shows a Gaussian shape for the noise of the VirConv detector across x and y LiDAR coordinates, which facilitates its integration into KF. Accordingly, we derive the 2×2 covariance matrix D_t representing the noise impact on the detections (measurements). Notably, the noise varies from one detector to another as to the variance in detection performance; hence, D_t should be recomputed as the employed detector changes. By applying Equation 1 on y coordinate, we obtain a covariance matrix of the noise, Equation 2.

$$\mathbf{D}_t = \begin{bmatrix} \sigma_x^2 & 0 \\ 0 & \sigma_y^2 \end{bmatrix} \quad (2)$$

Since this noise is attached to the incoming detections z_t at time t , it harms the computation of the residual term \hat{y}_t , which is the difference between the current measurement z_t and state estimation $\hat{x}_{t|t-1}$ predicted at $t - 1$. Consequently, the noise impact on the residual term leads to incorrect updates for the motion parameters of the object. The innovation covariance S_t is responsible for weighting the innovation residual \hat{y}_t through the Kalman gain K_t . Therefore, the covariance matrix D_t needs to be added to the innovation covariance S_t to compensate for the impact

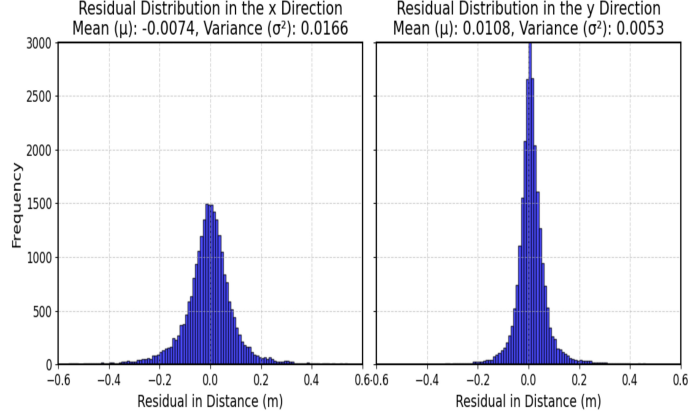


Figure 4: The distribution of the fluctuation noise associated with VirConv [19] detections. The distribution shows Gaussian noise across five different detectors [19, 20, 21, 22, 23].

of noise on the updated state. Hence, the updated state estimation $\hat{x}_{t|t}$ will consider the impact of the deviation noise on the observation.

$$\begin{aligned}
\text{Innovation Residual: } \tilde{y}_t &= z_t - H_t \hat{x}_{t|t-1} \\
\text{Innovation Covariance: } S_t &= H_t P_{t|t-1} H_t^T + R_t + D_t \\
\text{Kalman Gain: } K_t &= P_{t|t-1} H_t S_t^{-1} \\
\text{State Estimation Update: } \hat{x}_{t|t} &= \hat{x}_{t|t-1} + K_t \tilde{y}_t \\
\text{Estimation Covariance Update: } P_{t|t} &= (I - K_t H_t) P_{t|t-1}
\end{aligned} \tag{3}$$

The main reason for not using R_t instead is because it models the incorrectness of the measurement for the point cloud from LiDAR with respect to the real world, while D_t models the incorrectness of the detection process with respect to the LiDAR point cloud, which means they are independent. Equation 3 demonstrates the updated state of KF after adapting D_t noise.

H_t is the observation model to map from estimation to measurement space at time t , while $P_{t|t-1}$ is the estimation uncertainty at time t given measurement at $t - 1$. In Section 2.4, we will describe how $P_{t|t}$ contribute to trajectory termination in the cache.

2.3 Trajectory Validity

The objective is to monitor the validity (legitimacy) of the existing trajectories in the system while identifying invalid ones, called ghost tracks. Each track has a certainty score that represents its legitimacy. This score is updated whenever a new observation of the track is available. The certainty score changes based on the likelihood of the trajectory being a ghost track. By observing the characteristics of ghost tracks, the ghost tracks are usually formed from intermittent sequences of observations with low to moderate detection scores. Based on these characteristics, the certainty score for track i changes when a new observation is associated with the track at time t . The certainty score changes according to the detection score s_t^i and the duration of absence d_t^i since the last observation associated with the track.

- s_t^i : detection score of the current observation associated with track i at time t
- d_t^i : absence duration since the last associated observation at time k to track i and the current observation at time t
- k : The time stamp of the last associated observation to a trajectory
- $f_t^i(s_t^i, d_t^i)$: certainty score of trajectory i at time t
- $f_k^i(s_k^i, d_k^i)$: certainty score of trajectory i at time k

$$f_t^i(s_t^i, d_t^i) = s_t^i e^{-d_t^i} - \frac{d_t^i}{s_t^i} + f_k^i(s_k^i, d_k^i), \text{ where } s_t^i > 0$$

$$d_t^i = t - (k + 1)$$
(4)

As shown in Equation 4, the formulation consists of three terms: **Confidence decay** term $s_t^i e^{-d_t^i}$ (reward), **Absence duration** term (penalty) $\frac{d_t^i}{s_t^i}$, and **Temporal validity** $f_k^i(s_k^i, d_k^i)$ term.

2.3.1 Confidence decay

The term is responsible for increasing the certainty score of track i as the detection score s_t^i of the associated observation increases as a reward, indicating the detection model’s confidence in this observation. However, ghost tracks with moderate detection scores can receive high rewards, potentially misleading the validation mechanism. Thus, a decay rate, $e^{-d_t^i}$, is attached to the detection score s_t^i . The decay $e^{-d_t^i}$ increases as the duration d_t^i of the current observation at time t to the previous observation at time k increases. Given the intermittent characteristic of ghost tracks, the decay term decreases the detection score for potential ghost tracks in the system.

2.3.2 Absence duration

The penalty term $\frac{d_t^i}{s_t^i}$ lowers the certainty score as the absence duration d_t^i of a new observation for the track increases. This term will diminish the impact of the reward with an extended absence duration that indicates a high potential of being a ghost trajectory. However, this term can harm legitimate tracks that encounter occlusion. Since observations of legitimate tracks tend to have high detection scores s_t^i , we include inverse proportional to the detection score to decrease the impact of this term on the legitimate tracks.

2.3.3 Temporal validity

The inclusion of $f_k^i(s_k^i, d_k^i)$ integrates the previous certainty score calculated at time k to the current certainty score $f_t^i(s_t^i, d_t^i)$ of time t . This term adds temporal validation for trajectories in the system by incorporating historical certainty into the current certainty score so that $f_t^i(s_t^i, d_t^i)$ represents a certainty score of all trajectory states.

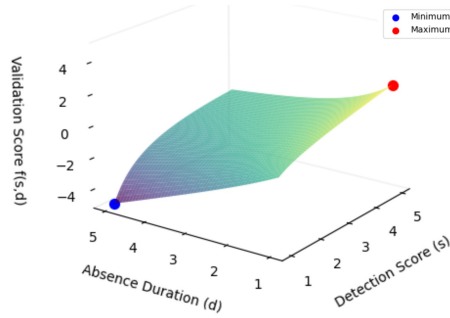


Figure 5: A graphical visualization of the certainty scoring formula over detection scores of range $[0, 5]$ and absence duration $[0, 5]$ frames. The **red point** is the highest certainty score when the detection score is highest while the absence duration is lowest. In contrast, the **blue point** is the lowest certainty score when the detection score is at the lowest value, while the absence duration is the highest. The surface shows the remaining values.

A visual representation of the distribution of Equation 4 is highlighted in Figure 5; the relation between the detection score, the absence duration, and its impact on the certainty score.

This mechanism monitors the validity of trajectories in the system individually until a certainty score of a trajectory exceeds a pre-defined threshold α_{legit} that indicates the trajectory is legitimate. In this case, the validation mechanism changes the trajectory status from “not confirmed” to “confirmed” and terminates the validation mechanism to this trajectory. Thus, confirmed trajectories cannot be changed to “not confirmed” as the mechanism is terminated for these tracks. Algorithm 2 demonstrates trajectory validation procedures in detail.

Algorithm 2 Trajectory Validity

```

function UpdateTrajectoryCertainty( $T, \alpha_{legit}$ )
Input:
   $T$ : List of trajectories in the cache
   $\alpha_{legit}$ : Trajectory legitimacy threshold

for each  $traj$  in  $T$  do
  if  $traj.hasNewObservation()$  then
     $s_t \leftarrow traj.getObservation().detectionScore()$ 
     $d_t \leftarrow traj.getAbsenceDuration()$ 
     $f_k \leftarrow traj.getCertaintyScore()$ 
     $f_t = s_t e^{-d_t} - \frac{d_t}{s_t} + f_k$ 
     $traj.setCertaintyScore(f_t)$ 

    if  $traj.getCertaintyScore() \leq \alpha_{legit}$  then
       $traj.setValidityStatus(true)$ 
    end if
  end if
end for
end function

```

2.4 Trajectory Termination and Caching

All trajectories are saved in a cache module. In the literature, a trajectory is terminated or discarded when there are no further observations for that trajectory for several frames. Generally, it is not trivial to define an absence threshold as it could risk eliminating objects under prolonged occlusion or maintaining ghost tracks for a long. Instead, in our framework, we discard the trajectory when the estimation uncertainty, $P_{t|t}$ in Equation 3, becomes high, as it can lead to mismatching in object association. We have observed that ghost tracks tend to have limited observations, leading to high uncertainty in state estimation that matches the intended goal. Meanwhile, legitimate tracks maintain low estimation uncertainty, even those under occlusion. Thus, estimation uncertainty is used to terminate tracks from the cache. Algorithm 3 demonstrates the termination procedures in the cache.

Algorithm 3 Trajectory Termination

```

function trajectory Termination( $T, \alpha_{cov}$ )
Input:
   $T$ : List of trajectories in the cache
   $\alpha_{cov}$ : Estimation uncertainty threshold to terminate a trajectory

for each  $traj$  in  $T$  do
   $estCertaintyX \leftarrow traj.getCovariance.P(0)$ 
   $estCertaintyY \leftarrow traj.getCovariance.P(1)$ 
   $discard \leftarrow false$ 
  if  $estCertaintyX > \alpha_{cov}$  then
     $discard \leftarrow true$ 
  end if
  if  $estCertaintyY > \alpha_{cov}$  then
     $discard \leftarrow true$ 
  end if
  if  $discard$  then
    Discard  $traj$  from  $T$ 
  end if
end for
end function

```

3 Results and Discussion

The framework is evaluated using two benchmark datasets for autonomous cars: KITTI [24] and Waymo Open Dataset [25] (WOD). The KITTI dataset consists of 50 sequences, split into 21 training sequences and 29 testing sequences recorded around Karlsruhe, Germany, that involve a variety of challenging conditions. Meanwhile, WOD contains about 1150 segments recorded in various locations across the United States. The experiments are conducted on a machine with a processor *AMD Ryzen 9*; no GPU is involved since the framework only utilizes the CPU.

The evaluation of the proposed approach consists of an extensive quantitative and qualitative evaluation with recent benchmarks in this section and a sensitive analysis of each proposed component to evaluate its contribution to the tracking performance, which will be covered in the ablation study, Section 3.2.

3.1 Evaluation with Benchmarks

This section consists of quantitative tracking performance evaluation with the latest state-of-the-art MOT methods on KITTI and WOD datasets and qualitative evaluation focusing on challenging occlusion conditions with the top-performing benchmark selected from the quantitative evaluation.

3.1.1 Quantitative Evaluation

Table 1: The table compares the latest benchmarks listed in the KITTI leaderboard on the testing split. The highest performance at each metric is highlighted in **red**, the second highest in **blue**, and the third highest in **green**. Methods that use the CasA [20] detector are marked by (*), while (+) is used for methods that use the VirConv [19] detector.

Method	HOTA	MOTA	AssA	AssRe	IDSW
TripletTrack [26]	73.58%	84.32%	74.66%	77.3%	322
PolarMOT [27]	75.2%	85.1%	76.95%	80.0%	462
DeepFusion-MOT [2]	75.5%	84.6%	80.1%	82.6%	84
Mono-3D-KF [28]	75.5%	88.5%	77.6%	80.2%	162
PC3T [29]	77.8%	88.8%	81.6%	84.8%	225
MSA-MOT [30]	78.5%	88.0%	82.6%	85.2%	91
UG3DMOT* [31]	78.6%	87.98%	82.28%	85.36%	30
CasTrack* [1]	80%	90.5%	82.7%	86.4%	150
Rethink MOT [5]	80.1%	91.5%	83.6%	87.6%	46
MCTrack [32]	80.78%	89.82%	84.29%	-	65
PC-TCNN [33]	80.9%	91.7%	84.1%	87.5%	37
VirConvTrack+ [19, 1]	81.56%	90.54%	85.2%	88.7%	113
RobMOT* (Ours)	81.22%	90.5%	85.8%	89.7%	7
RobMOT+ (Ours)	81.76%	91.02%	85.6%	89.25%	7

We evaluate the performance of the proposed framework, RobMOT [?], against several state-of-the-art multi-object tracking benchmarks on the KITTI dataset testing split. The results are summarized in Table 1, which presents metrics: HOTA (Higher Order Tracking Accuracy), MOTA (Multi-Object Tracking Accuracy), AssA (Association Accuracy), AssRe (Association Recall), and IDSW (Identity Switches).

In this comparison, we use two different detectors, VirConv [19] and CasA [20], to evaluate the tracking performance rather than the detection fairly. We are re-running the official implementation of the CasTrack [1] work as it is the latest top-performing classical approach using their proposed detectors CasA [20] and VirConv [19]. Our proposed framework, RobMOT, outperforms CasTrack with the CasA detector, marked by (*) in Table 1, with about 1.22% in HOTA. By switching the detector to VirConv, our method still outperforms CasTrack [1], named "VirConvTrack" [19] in Table 1, with about 0.2% in HOTA, marked by (+) in Table 1. These results show the contribution of the proposed tracking approach regardless of the performance of the utilized detector. Notably, RobMOT is ranked the first or second highest in most metrics, with CasA or VirConv detector among the other benchmarks. In addition, the proposed work excels in Association Accuracy (AssA) with 85.8%, marking it the highest among the evaluated methods. Similarly, it achieves a leading Association Recall (AssRe) of 89.7%, indicating its robust capability to maintain correct identity associations throughout the tracking process.

One of the most significant contribution is the low Identity Switches (IDSW) score of 7 for RobMOT with CasA and VirConv detectors. This demonstrates the model’s ability to consistently track object identities over time, which

is critical for reliable multi-object tracking. In contrast, other benchmark methods, such as UG3DMOT [31] and CasTrack [1] with the same detector, exhibit substantially higher IDSW scores of 30 and 150, respectively, indicating more frequent identity switches.

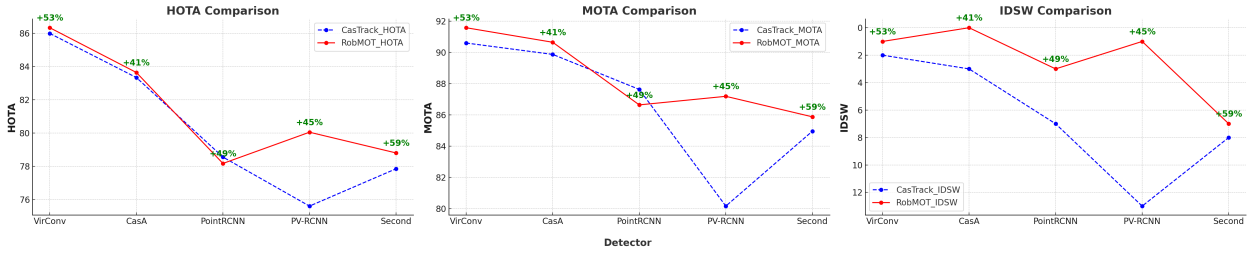


Figure 6: Tracking performance comparison on KITTI dataset *validation split* with CasTrack [1] across five different detectors: VirConv [19], CasA [20], PointRCNN [22], PV-RCNN [23], and Second [21]. RobMOT (in red) consistently outperforms CasTrack (in blue) across all detectors, with significant improvements in both HOTA and MOTA metrics, particularly with the PV-RCNN detector, and a substantial reduction in IDSW. Additionally, RobMOT demonstrates a minimum 40% increase in processing speed (fps) across all detectors, highlighting its efficiency and robustness. The percentage improvements are indicated in green.

Our further experiments on the KITTI evaluation dataset across five detectors show CasTrack [1] and VirConvTrack [19] dependency on the utilized detector, as illustrated in Figure 6. It shows the tracking performance across the detectors using three different metrics: MOTA, HOTA, and IDSW. Although both methods show close performance in HOTA and MOTA with VirConv [19], CasA [20], and PointRCNN [22], CasTrack [1] performance drops dramatically in PV-RCNN [23] with a margin of more than 6% in MOTA and 4% in HOTA.

Our proposed method, while maintaining the lowest IDSW compared to CasTrack [1], consistently outperforms across all detectors. These results validate the contribution of the proposed tracking approach, demonstrating its exceptional performance across various detectors. Additionally, the proposed approach achieves higher frame per second (fps) than CasTrack [1] across the detectors, with an fps enhancement reaching +59% with the Second [21] detector.

Another evaluation is conducted on the WOD testing dataset to measure the generalization of the approach. The dataset consists of simple to moderate tracking conditions labeled “Level 1” and challenging conditions labeled “Level 2” in Table 2. Our proposed solution shows superior tracking performance on the recent benchmark, including CasTrack [1], with a reduction in the false positives ratio (FP).

Table 2: Tracking performance on Waymo Open dataset *testing split* with the latest MOT benchmarks. Methods that use the CasA [20] detector are marked by (*)

Method	Level 1		Level 2	
	MOTA↑	FP↓	MOTA↑	FP↓
CasTrack* [1]	66.95%	7.74%	63.66%	7.36%
ImmotralTrack [34]	63.77%	8.94%	60.55%	8.48%
SimpleTrack [35]	63.53%	8.66%	60.30%	8.75%
CenterPoint [36]	62.58%	9.03%	59.38%	9.41%
AlphaTrack [37]	58.86%	10.10%	55.67%	9.55%
RobMOT* (Ours)	67.02%	7.60%	63.67%	7.22%

In conclusion, the proposed approach excels in tracking stability and accuracy, significantly reducing ID switches and enhancing fps performance across various detectors. It outperforms recent state-of-the-art methods like CasTrack [1] on both the KITTI and WOD datasets, demonstrating robust generalization and efficiency. The quantitative results validate the contribution and exceptional performance of the proposed framework.

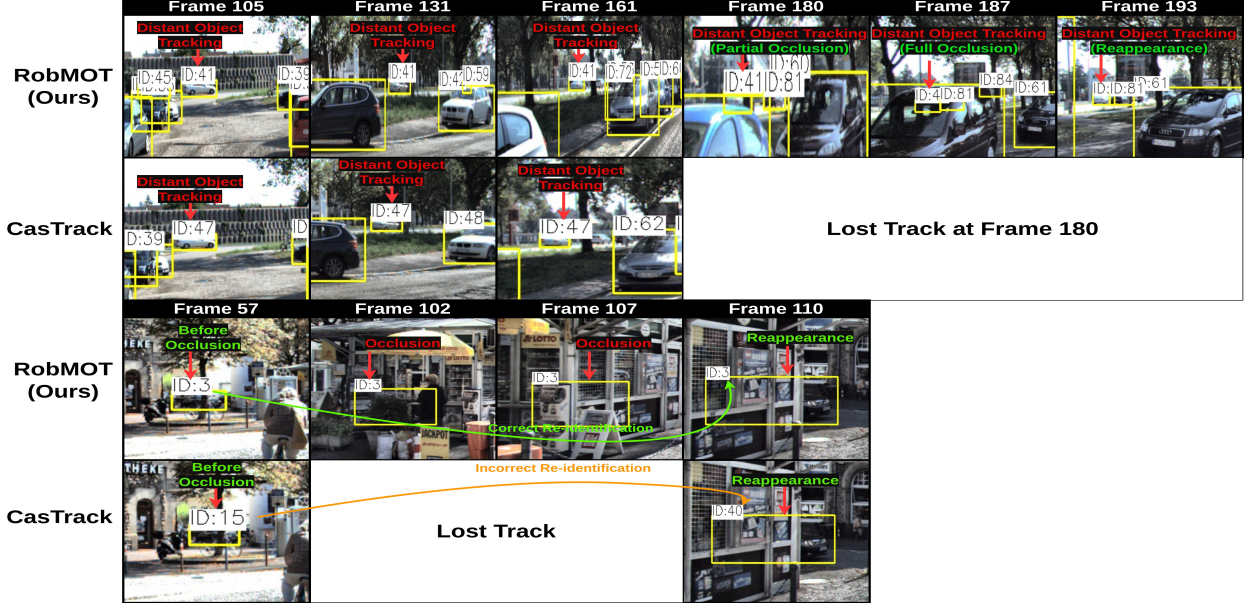


Figure 7: A qualitative evaluation of our framework performance with CasTrack [1] in two challenging multi-object tracking scenarios by projecting 3D tracking results into 2D frames. The first two rows show a scenario where a distant car ($ID:41$) faces multiple occlusions and distortion in detection. The second two rows show a scenario of a car ($ID:3$) occluded by a building for about 50 consecutive frames. Our framework tracks the distant car in the first scenario under distortion in the observation and occlusions while providing precise state estimation of the prolonged occluded car in the second scenario with successful recovery after the occlusion.

3.1.2 Qualitative Evaluation

Although the quantitative evaluation shows the overall performance of a tracking approach, it is not sufficient to evaluate the method under challenging tracking conditions such as occlusions. Thus, we select two challenging conditions to emphasize the contribution of the proposed approach. The first condition represented in the first two rows in Figure 7 is for a distant car that faces frequent occlusions for about 90 frames. The detector is unified for both methods, ours and CasTrack [1], to measure the contribution of the tracking approach. Our proposed solution maintains tracking for the car with ID 41 to frame 193 when the car leaves the field of view of LiDAR, while CasTrack [1] lost the car at frame 180.

Another challenging scenario is illustrated in Figure 7 in the third and fourth rows. In frame 57, a distant car behind a tree is occluded by a building in the following frames until frame 110, when the car partially appears again. Our proposed method shows robustness in state estimation of the car during occlusion, as shown in frames 102 and 107, and successfully reassociates the car when it appears in frame 110. On the other hand, CasTrack [1] loses track of the car during the occlusion and considers the re-appearance of the car as a new car associated with a new trajectory.

The two scenarios show the robustness of the proposed approach and capability to handle challenging occlusion scenarios compared to the recent state-of-the-art CasTrack [1].

3.2 Ablation Study

This section will cover a sensitivity analysis conducted on the proposed method to show the contribution of each component proposed in this work and quantitatively measure its impact on tracking performance.

3.2.1 Trajectory Drift

This research raises concerns about noise injected in the incoming detections, which leads to deviation in the state estimation of objects during occlusion. The noise is observed in multiple scenarios (Figure 3) and the recent state-of-the-art method CasTrack [1] (Figure 1), which emphasizes the existence of this problem. This section demonstrates

the quantitative impact of this noise on the tracking performance and the contribution of the proposed noise mitigation approach discussed in this work in improving the performance by mitigating the noise.

Table 3: Performance comparison of different detectors with and without the proposed refinement for noise mitigation D_t .

Metric	D_t	VirConv	CasA	PointRCNN	PV-RCNN	Second
HOTA	Y	83%	80.5%	75.7%	78.1%	76.6%
	N	80.5%	77.2%	72.1%	73.4%	73.5%
Improvement	-	+2.5%	+3.3%	+3.6%	+4.7%	+3.1%
MOTA	Y	87.2%	86.4%	81.5%	84.2%	83.2%
	N	82.4%	80.8%	76%	77.6%	78.8%
Improvement	-	+4.8%	+5.6%	+5.5%	+6.6%	+4.4%
IDSW	Y	8	4	11	9	8
	N	11	19	40	44	33
Improvement	-	-3	-15	-29	-35	-25
MT	Y	479	509	501	496	492
	N	470	498	477	484	483
Improvement	-	+9	+11	+24	+12	+9

In this experiment, we compare the performance of the Kalman filter without the proposed refinement for noise mitigation, D_t , and the contribution by including the refined Kalman filter. The experiment is conducted on five different detectors to justify the contribution of the proposed refinement Kalman filter, as demonstrated in Table 3. The comparison focuses on metrics MOTA, HOTA, IDSW, and the number of mostly tracked objects (MT). Since our method is not a learning approach, the evaluation is conducted on the KITTI training and evaluation dataset of 21 streams in total. The proposed refinement in Kalman filter consistently enhances the tracking performance across the five detectors, as shown in Table 3. The improvement in HOTA reached 4.7% with PV-RCNN [23] detector and 6.6% in MOTA. Moreover, it shows consistent state estimation for trajectories that lead to fewer ID switches (IDSW), reduction by 35 IDs, and more tracked objects (MT); about 24 objects increased with the PointRCNN [22] detector.

These results, including the qualitative results represented in this work, confirm the contribution of the proposed Kalman filter refinement that mitigates the noise associated with the detections, enhancing state estimation and tracking performance.

3.2.2 Track Validity and Ghost Tracks

The second concern raised in this research is ghost tracks. Ghost tracks are a form of consecutive false positive observations that generate illusion trajectories that could mislead MOT methods. This work proposes an online trajectory validation mechanism to identify ghost tracks among legitimate trajectories in the system. We validate the contribution of the proposed mechanism in two steps. First, we demonstrate a qualitative scenario where ghost and legitimate tracks exist and the capability of the mechanism to identify legitimate tracks. Second, we perform a sensitivity analysis by disabling the mechanism and quantifying the improvement in the tracking performance.

Figure 8 reports a qualitative experiment of the trajectory validation mechanism for identifying legitimate tracks. The figure shows a scenario of three legitimate tracks for three cars with ID 49, 48, and 0 and two ghost tracks with ID 50 and 48 at frame 277. A car with ID 47 is identified as a legitimate track at frame 279, while the car with ID 49 is confirmed at frame 285. The ghost tracks with ID 49, 48, and 0 remain unconfirmed until discarded from the system. This scenario shows the capability of the mechanism to identify legitimate tracks among ghost tracks.

To support the proposed trajectory validity mechanism’s impact on tracking performance, we disable the mechanism and quantitatively evaluate the tracking performance on the training and evaluation KITTI dataset. To demonstrate the generalization of the proposed mechanism, we employ five different detectors and quantify the enhancement in performance across five detectors when the trajectory validity mechanism is enabled. While the trajectory validity mechanism is disabled, we employ threshold on the detection score as proposed and fine-tuned in CasTrack [1] work. The evaluation involves HOTA, MOTA, and IDSW metrics to represent the overall tracking performance. Table 4 shows that enabling the trajectory validity mechanism improves HOTA across all detectors, with a margin reaching

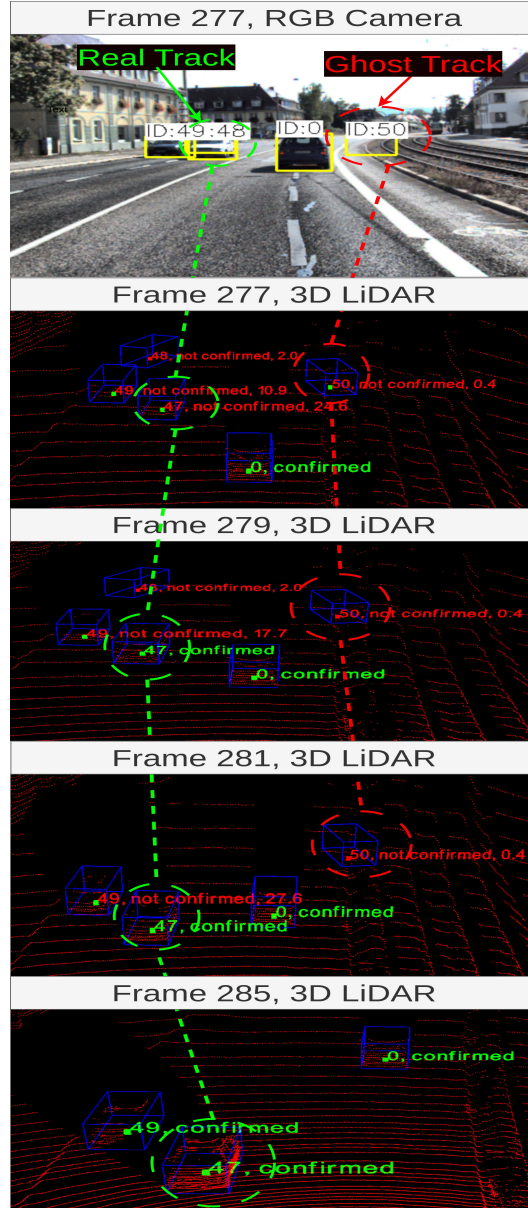


Figure 8: This scenario illustrates the proposed trajectory validity mechanism’s capability of distinguishing between real tracks (Car ID:47, Car ID:49) and ghost tracks (Car ID:48, Car ID: 50). It showcases the ability to accurately identify and maintain a ‘Not Confirmed’ status for the ghost track while recognizing Car ID:49 and Car ID:47 as legitimate tracks.

6.28% with PointRCNN [22] detector. Moreover, there is a significant improvement in the multi-object tracking accuracy (MOTA) metric for overall detectors that peak with the PointRCNN detector with up to 17.87% enhancement in MOTA. Since the trajectory validity mechanism identifies legitimate tracks while allowing their observations to pass through the system, the tracking performance becomes more consistent with less misidentification for objects that reflect few IDSW values, as shown in Table 4. It results in a reduction in IDSW reaches 56 with PV-RCNN [23] detector.

The combination of the qualitative results in Figure 8 and the quantitative results in Table 4 confirms the contribution of the proposed mechanism to object tracking performance.

Table 4: Performance evaluation of our framework with and without the proposed trajectory validity mechanism across five detectors

Detector	Traj. Validity	HOTA \uparrow	MOTA \uparrow	IDSW \downarrow
PointRCNN [22]	N	69.38%	63.59%	58
PointRCNN [22]	Y	75.66%	81.46%	11
Improvement	-	+6.28%	+17.87%	-47
PV-RCNN [23]	N	73.92%	73.72%	65
PV-RCNN [23]	Y	78.13%	84.2%	9
Improvement	-	+4.21%	+10.45%	-56
Second [21]	N	73.69%	75.78%	39
Second [21]	Y	76.64%	83.22%	8
Improvement	-	+2.95%	+7.44%	-31
CasA [20]	N	78.28%	80.75%	26
CasA [20]	Y	80.53%	86.36%	4
Improvement	-	+2.25%	+5.61%	-22
VirConv [19]	N	80.66%	83.03%	21
VirConv [19]	Y	83.01%	87.17%	8
Improvement	-	+2.35%	+4.14%	-13

4 Conclusion

This paper discusses two critical challenges in multi-object tracking (MOT): state estimation deviation and ghost tracks. Our research reveals that the noise associated with detections from the detector affects the accuracy of bounding box localization, leading to errors in estimating the motion parameters of these objects. This problem causes trajectory estimation to drift, particularly when objects encounter occlusion, and has been noted in recent advanced MOT methods. Another type of noise is formed from false positive observations that lead to ghost tracks. While the literature relies on fine-tuned thresholds on the detection score to filter observations contributing to these tracks, it still leaks false observations and blocks observation of legitimate tracks, eventually impacting tracking performance. We addressed this issue with a refined Kalman filter compensating for trajectory drift noise, allowing drift mitigation, and recovering prolonged occluded objects. The work also introduces a novel online trajectory validity mechanism to identify legitimate tracks based on ghost track characteristics in MOT methods.

The proposed solutions are combined in an online MOT framework, RobMOT, that outperforms state-of-the-art trackers in KITTI and Waymo Open Dataset. The framework shows superior tracking performance across various detectors with a margin reaching 4% in HOTA and 6% in MOTA with the top-performing MOT benchmark. The framework qualitatively shows its substantial tracking performance for distant and recovering prolonged occluded objects when SOTA fails. An ablation study has been conducted to demonstrate the improvement in the tracking performance resulting from each component proposed in this work. The study shows that mitigation of the state estimation drift noise enhances HOTA by 4.7% and MOTA by 6.6%. Meanwhile, the proposed trajectory validity mechanism significantly improves the tracking performance, reaching 6.28% in HOTA and 17.87% in MOTA, dramatically reducing the IDSW metric to 56 IDs. The framework shows its applicability to real-time solutions with CPU constraints and high computational processing.

A Thresholds and Parameter Values

Table 5: List of Thresholds and Parameter Values

Detector	$D_t(\sigma_x^2)$	$D_t(\sigma_y^2)$	σ_{nconf}	σ_{conf}	σ_{legit}	σ_{conv}
VirConv [19]	0.016629	0.005334	0	-1	20	4
CasA [20]	0.030696	0.015416	0	0	25	4
PointRCNN [22]	0.032043	0.009945	0	0	35	4
PV-RCNN [23]	0.034076	0.012463	0.5	0.5	20	4
Second [21]	0.037623	0.013561	-1	-2	10	4

References

- [1] Wu et al. 3d multi-object tracking in point clouds based on prediction confidence-guided data association. *IEEE Transactions on Intelligent Transportation Systems*, 2022.
- [2] Xiyang Wang, Chunyun Fu, Zhankun Li, Ying Lai, and Jiawei He. Deepfusionmot: A 3d multi-object tracking framework based on camera-lidar fusion with deep association. *IEEE Robotics and Automation Letters*, 7(3):8260–8267, 2022.
- [3] Aleksandr Kim, Aljoša Ošep, and Laura Leal-Taixé. Eagermot: 3d multi-object tracking via sensor fusion. In *2021 IEEE International Conference on Robotics and Automation (ICRA)*, pages 11315–11321, 2021.
- [4] Liang Hu, Taihui Li, Nannan Xie, and Jiejun Hu. False positive elimination in intrusion detection based on clustering. In *2015 12th International Conference on Fuzzy Systems and Knowledge Discovery (FSKD)*, pages 519–523, 2015.
- [5] Leichen Wang, Jiadi Zhang, Pei Cai, and Xinrun Lil. Towards robust reference system for autonomous driving: Rethinking 3d mot. In *2023 IEEE International Conference on Robotics and Automation (ICRA)*, pages 8319–8325, 2023.
- [6] Jinkun Cao, Jiangmiao Pang, Xinshuo Weng, Rawal Khirodkar, and Kris Kitani. Observation-centric sort: Rethinking sort for robust multi-object tracking. In *Proceedings of the IEEE/CVF Conference on Computer Vision and Pattern Recognition (CVPR)*, pages 9686–9696, June 2023.
- [7] Kaer Huang, Kanokphan Lertniphonphan, Feng Chen, Jian Li, and Zhepeng Wang. Multi-object tracking by self-supervised learning appearance model. In *Proceedings of the IEEE/CVF Conference on Computer Vision and Pattern Recognition*, pages 3162–3168, 2023.
- [8] Jiarui Cai, Mingze Xu, Wei Li, Yuanjun Xiong, Wei Xia, Zhuowen Tu, and Stefano Soatto. Memot: Multi-object tracking with memory. In *Proceedings of the IEEE/CVF Conference on Computer Vision and Pattern Recognition*, pages 8090–8100, 2022.
- [9] Pavel Tokmakov, Jie Li, Wolfram Burgard, and Adrien Gaidon. Learning to track with object permanence. In *Proceedings of the IEEE/CVF International Conference on Computer Vision*, pages 10860–10869, 2021.
- [10] Tim Meinhardt, Alexander Kirillov, Laura Leal-Taixé, and Christoph Feichtenhofer. Trackformer: Multi-object tracking with transformers. In *Proceedings of the IEEE/CVF conference on computer vision and pattern recognition*, pages 8844–8854, 2022.
- [11] Chaoda Zheng, Xu Yan, Haiming Zhang, Baoyuan Wang, Shenghui Cheng, Shuguang Cui, and Zhen Li. Beyond 3d siamese tracking: A motion-centric paradigm for 3d single object tracking in point clouds. In *Proceedings of the IEEE/CVF Conference on Computer Vision and Pattern Recognition*, pages 8111–8120, 2022.
- [12] Jeongseok Hyun, Myunggu Kang, Dongyoon Wee, and Dit-Yan Yeung. Detection recovery in online multi-object tracking with sparse graph tracker. In *Proceedings of the IEEE/CVF Winter Conference on Applications of Computer Vision*, pages 4850–4859, 2023.
- [13] Gianluca Mancusi, Aniello Panariello, Angelo Porrello, Matteo Fabbri, Simone Calderara, and Rita Cucchiara. Trackflow: Multi-object tracking with normalizing flows. In *Proceedings of the IEEE/CVF International Conference on Computer Vision*, pages 9531–9543, 2023.
- [14] Yuang Zhang, Tiancai Wang, and Xiangyu Zhang. Motrv2: Bootstrapping end-to-end multi-object tracking by pretrained object detectors. In *Proceedings of the IEEE/CVF Conference on Computer Vision and Pattern Recognition*, pages 22056–22065, 2023.

- [15] Kaer Huang, Kanokphan Lertniphonphan, Feng Chen, Jian Li, and Zhepeng Wang. Multi-object tracking by self-supervised learning appearance model. In *2023 IEEE/CVF Conference on Computer Vision and Pattern Recognition Workshops (CVPRW)*, pages 3163–3169, 2023.
- [16] Gianluca Mancusi, Aniello Panariello, Angelo Porrello, Matteo Fabbri, Simone Calderara, and Rita Cucchiara. Trackflow: Multi-object tracking with normalizing flows. In *Proceedings of the IEEE/CVF International Conference on Computer Vision (ICCV)*, pages 9531–9543, October 2023.
- [17] Mohamed Nagy, Majid Khonji, Jorge Dias, and Sajid Javed. Dfr-fastmot: Detection failure resistant tracker for fast multi-object tracking based on sensor fusion. In *2023 IEEE International Conference on Robotics and Automation (ICRA)*, pages 827–833, 2023.
- [18] Harold W Kuhn. The hungarian method for the assignment problem. *Naval research logistics quarterly*, 2(1-2):83–97, 1955.
- [19] Wu et al. Virtual sparse convolution for multimodal 3d object detection. In *Proceedings of the IEEE/CVF Conference on Computer Vision and Pattern Recognition (CVPR)*, June 2023.
- [20] Wu et al. Casa: A cascade attention network for 3-d object detection from lidar point clouds. *IEEE Transactions on Geoscience and Remote Sensing*, 2022.
- [21] Yan Yan, Yuxing Mao, and Bo Li. Second: Sparsely embedded convolutional detection. *Sensors*, 18(10):3337, 2018.
- [22] Shaoshuai Shi, Xiaogang Wang, and Hongsheng Li. Pointcnn: 3d object proposal generation and detection from point cloud. In *The IEEE Conference on Computer Vision and Pattern Recognition (CVPR)*, June 2019.
- [23] Shaoshuai Shi, Chaoxu Guo, Li Jiang, Zhe Wang, Jianping Shi, Xiaogang Wang, and Hongsheng Li. Pv-rcnn: Point-voxel feature set abstraction for 3d object detection. In *Proceedings of the IEEE/CVF Conference on Computer Vision and Pattern Recognition (CVPR)*, June 2020.
- [24] Andreas Geiger, Philip Lenz, and Raquel Urtasun. Are we ready for autonomous driving? the kitti vision benchmark suite. In *Conference on Computer Vision and Pattern Recognition (CVPR)*, 2012.
- [25] Pei Sun, Henrik Kretschmar, Xerxes Dotiwalla, Aurélien Chouard, Vijaysai Patnaik, Paul Tsui, James Guo, Yin Zhou, Yuning Chai, Benjamin Caine, Vijay Vasudevan, Wei Han, Jiquan Ngiam, Hang Zhao, Aleksei Timofeev, Scott Ettinger, Maxim Krivokon, Amy Gao, Aditya Joshi, Yu Zhang, Jonathon Shlens, Zhifeng Chen, and Dragomir Anguelov. Scalability in perception for autonomous driving: Waymo open dataset. In *2020 IEEE/CVF Conference on Computer Vision and Pattern Recognition (CVPR)*, pages 2443–2451, 2020.
- [26] Nicola Marinello, Marc Proesmans, and Luc Van Gool. Triplettrack: 3d object tracking using triplet embeddings and lstm. In *Proceedings of the IEEE/CVF Conference on Computer Vision and Pattern Recognition*, pages 4500–4510, 2022.
- [27] Aleksandr Kim, Guillem Brasó, Aljoša Ošep, and Laura Leal-Taixé. Polarmot: How far can geometric relations take us in 3d multi-object tracking? In Shai Avidan, Gabriel Brostow, Moustapha Cissé, Giovanni Maria Farinella, and Tal Hassner, editors, *Computer Vision – ECCV 2022*, pages 41–58, Cham, 2022. Springer Nature Switzerland.
- [28] Andreas Reich and Hans-Joachim Wuensche. Monocular 3d multi-object tracking with an ekf approach for long-term stable tracks. In *2021 IEEE 24th International Conference on Information Fusion (FUSION)*, pages 1–7, 2021.
- [29] Hai Wu, Wenkai Han, Chenglu Wen, Xin Li, and Cheng Wang. 3d multi-object tracking in point clouds based on prediction confidence-guided data association. *IEEE Transactions on Intelligent Transportation Systems*, 23(6):5668–5677, 2022.
- [30] Ziming Zhu, Jiahao Nie, Han Wu, Zhiwei He, and Mingyu Gao. Msa-mot: Multi-stage association for 3d multimodality multi-object tracking. *Sensors*, 22(22):8650, 2022.
- [31] Jiawei He, Chunyun Fu, Xiyang Wang, and Jianwen Wang. 3d multi-object tracking based on informatic divergence-guided data association. *Signal Processing*, 222:109544, 2024.
- [32] Xiyang Wang, Shouzheng Qi, Jieyou Zhao, Hangning Zhou, Siyu Zhang, Guoan Wang, Kai Tu, Songlin Guo, Jianbo Zhao, Jian Li, and Mu Yang. Mctrack: A unified 3d multi-object tracking framework for autonomous driving, 2024.
- [33] Hai Wu, Qing Li, Chenglu Wen, Xin Li, Xiaoliang Fan, and Cheng Wang. Tracklet proposal network for multi-object tracking on point clouds. In Zhi-Hua Zhou, editor, *Proceedings of the Thirtieth International Joint Conference on Artificial Intelligence, IJCAI-21*, pages 1165–1171. International Joint Conferences on Artificial Intelligence Organization, 8 2021. Main Track.

- [34] Qitai Wang, Yuntao Chen, Ziqi Pang, Naiyan Wang, and Zhaoxiang Zhang. Immortal tracker: Tracklet never dies. *arXiv preprint arXiv:2111.13672*, 2021.
- [35] Ziqi Pang, Zhichao Li, and Naiyan Wang. Simpletrack: Understanding and rethinking 3d multi-object tracking. In *ECCV Workshops*, 2021.
- [36] Tianwei Yin, Xingyi Zhou, and Philipp Krahenbuhl. Center-based 3d object detection and tracking. In *Proceedings of the IEEE/CVF Conference on Computer Vision and Pattern Recognition (CVPR)*, pages 11784–11793, June 2021.
- [37] Yihan Zeng, Chao Ma, Ming Zhu, Zhiming Fan, and Xiaokang Yang. Cross-modal 3d object detection and tracking for auto-driving. In *2021 IEEE/RSJ International Conference on Intelligent Robots and Systems (IROS)*, pages 3850–3857, 2021.